AIAA 81-0605R

Dynamics of a Flexible Cylinder in Subsonic Axial Flow

Michael P. Paidoussis* and Martin Ostoja-Starzewski†
McGill University, Montreal, Québec, Canada

This paper examines the dynamics of a flexible cylinder with pinned ends immersed in axial subsonic flow, either bounded or unconfined. The problem proves to be surprisingly resistant to exact solution, as compared to the incompressible flow case, because of difficulties in determining precisely the inviscid aerodynamic forces. This paper presents a number of distinct formulations of these forces, involving different approximations: 1) a slender-body approximation; 2) an approximate three-dimensional formulation where, in the determination of the aerodynamic forces, the axial mode shape is prescribed in advance; and 3) an "exact" integral formulation of the generalized aerodynamic forces. In each case, Galerkin-type solutions yield the system eigenfrequencies which describe the dynamical behavior of the system. It is found that for sufficiently high flow velocities, divergence and flutter are possible. The different methods yield similar, but not quantitatively identical results. Interestingly, dependence of the dynamical characteristics on Mach number is shown to be weak for slender cylinders; for nonslender ones, it is stronger. Finally, a brief discussion of wave propagation in an unconstrained cylinder indicates the existence of a cutoff flow velocity for backward propagating waves, followed by wave amplification at higher flow, which is closely related to loss of stability in the constrained system.

I. Introduction

THE dynamics of a slender flexible cylinder in incompressible axial flow have been studied rather thoroughly[1-3] and, recently, theoretical and experimental study has been extended to deal with clusters of cylinders (for example, Ref. 4). Apart from their inherent interest, these studies are of interest to those concerned with flow-induced vibrations of heat-exchanger tubes and nuclear reactor fuel rods.

The present study was initiated in an attempt to explain why the behavior of a cylinder in single-phase flow, as observed in experiments conducted in water, was so radically different from that in two-phase (gas-liquid) flow, as discussed in Refs. 5 and 6. Suffice it to say here that theory predicts that these instabilities should occur for both single-phase and homogeneous incompressible two-phase flows; in the experiments, however, the instabilities were observed to occur only in single-phase flow and were totally absent in two-phase flows. Of course, two-phase flow is anything but incompressible; hence, the motivation of this study to examine the effect of compressibility on the dynamical behavior of the system. In this connection, it should be recalled that the sonic speed in two-phase mixtures can easily be one-tenth the sonic speed in either the liquid or the gas, and as low as one-fiftieth at low pressures[7]; this is because the two-phase mixture essentially has the massiveness of the liquid and compressibility of the gas.

Although this was the initial motivation for this study, the problem was quickly generalized so that what is presented here is a study of the dynamical behavior of a cylinder subjected to a subsonic axial flow, irrespective of whether the fluid is a gas or a homogeneous flow model of a two-phase mixture. Also, since all previous studies[1-4] obtained the aerodynamic forces by the slender-body approximation, the scope of this work was extended to attempt the formulation of these forces by three-dimensional flow theory, which proved to be less straightforward than anticipated.

Received Nov. 19, 1980; revision received April 8, 1981; presented as Paper 81-0605 at the AIAA Dynamics Specialists Conference, Atlanta, Ga., April 9-10, 1981.

*Professor and Chairman, Dept. of Mechanical Engineering.
†Research Assistant, Dept. of Mechanical Engineering. Student Member AIAA.

This paper presents various approaches to dealing with the problem. First, the problem is analyzed by the slender-body approximation. Then, an approximate three-dimensional theory is presented, followed by a more general integral approach, based on Dowell's[8,9] generalized-force formulation. In all cases, the cylinder extremities are supposed to be pinned (simply supported), except when discussing wave propagation, when the cylinder is free of end constraints. The flow is generally considered to be bounded by an external rigid channel, as shown in Fig. 1. It is further supposed that the flexible cylinder is attached to rigid, but otherwise identical, semi-infinite cylinders extending over $-\infty < x \leq 0$ and $L \leq x < \infty$ for analytical convenience.

II. Equation of Motion

The equation of small lateral motions of a cylinder in axial flow will not be derived here in full detail, since it can be found in Ref. 3. Modeling the cylinder as an Euler-Bernoulli beam of flexural rigidity EI, radius a, length L, cross-sectional area A, and mass per unit length m, and considering small lateral motions $v(x,t)$ in an arbitrary (r,x) plane, an element δx of the cylinder will be subjected to the following forces:

$EI(\partial^4 v/\partial x^4)\delta x$:	flexural restoring force
$F_A \delta x$:	lateral inviscid aerodynamic force
$F_N \delta x$:	normal viscous aerodynamic force
$F_L \delta x$:	longitudinal viscous aerodynamic force
$(\partial/\partial x)[(T+pA)(\partial v/\partial x)]$:	lateral force due to tension T on the cylinder and to fluid pressure p
$m(\partial^2 v/\partial t^2)$:	inertial force

Taking force and moment balances about the element δx, it is easy to obtain the equation

$$EI\frac{\partial^4 v}{\partial x^4} + F_A + F_N - \frac{\partial}{\partial x}\left[(T+pA)\frac{\partial v}{\partial x}\right] - F_L\frac{\partial v}{\partial x} + m\frac{\partial^2 v}{\partial t^2} = 0 \tag{1}$$

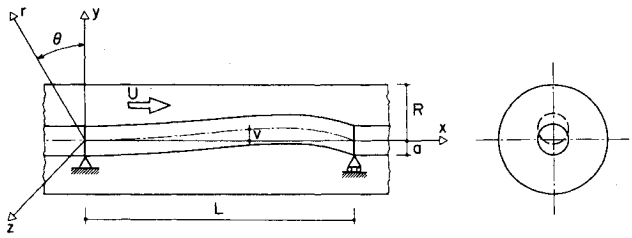

Fig. 1 Flexible slender cylinder in bounded axial flow.

where it is noted that internal dissipation in the material of the cylinder is not considered, for simplicity. The determination of the force F_A is considered to be the main concern of this paper, as will be discussed in the sections to follow. The other forces are considered to be unaffected by fluid compressibility and are given as follows.

The viscous forces are approximated by expressions first proposed by Taylor[3,10,11] for cylinders inclined to the flow. They are given by

$$F_N = \frac{1}{2}\rho D U^2 C_f \left[\left(\frac{\partial v}{\partial t} + U\frac{\partial v}{\partial x}\right)\Big/ U\right]^{\ddagger}$$

$$F_L = \frac{1}{2}\rho D U^2 C_f \tag{2}$$

where ρ is the fluid density, U the flow velocity, C_f the frictional coefficient, and D the cylinder diameter.

The form of the tension and pressure forces depends on whether one supposes the downstream end to be axially constrained or not. Assuming the latter, tension forces can only arise by the cumulative effect of F_L along the length. According to the simplifying assumptions of Ref. 3, one obtains

$$\frac{\partial}{\partial x}(T+pA) + F_L - \frac{\partial p}{\partial x}A = 0, \quad -A\frac{\partial p}{\partial x} = \frac{1}{2}\rho D U^2 C_f\left(\frac{D}{D_h}\right) \tag{3}$$

where D_h is the hydraulic diameter of the channel flow, and where gravity effects have been neglected.

By substituting Eqs. (2) and (3) into Eq. (1), the equation of small lateral motions is obtained

$$EI\frac{\partial^4 v}{\partial x^4} + F_A - \frac{1}{2}\rho D U^2 C_f\left(1+\frac{D}{D_h}\right)(L-x)\frac{\partial^2 v}{\partial x^2}$$

$$+\frac{1}{2}\rho D U^2 C_f\left(1+\frac{D}{D_h}\right)\frac{\partial v}{\partial x} + \frac{1}{2}\rho D U C_f\frac{\partial v}{\partial t} + m\frac{\partial^2 v}{\partial t^2} = 0 \tag{4}$$

subject to the boundary conditions

$$v(0,t) = v(L,t) = 0, \qquad \frac{\partial^2 v}{\partial x^2}\Big|_{x=0,L} = 0 \tag{5}$$

According to the slender-body approximation for an incompressible fluid, $F_A = M_h[(\partial^2 v/\partial t^2) + 2U(\partial^2 v/\partial x \partial t) + U^2(\partial^2 v/\partial x^2)]$, where M_h is the virtual (or "hydrodynamic") mass of the fluid; for unconfined flow $M_h = \rho A$, whereas for bounded flow,[3,4] $M_h > \rho A$. In Secs. III, IV, and V, F_A will be determined by different methods and the equations will then be solved in each case. Before doing so, Eqs. (4) and (5) will be nondimensionalized by use of the following parameters:

$$\xi = \frac{x}{L}, \quad \eta = \frac{v}{L}, \quad \beta = \frac{\rho A}{\rho A + m}$$

$$\tau = \left\{\frac{EI}{\rho A + m}\right\}^{1/2}\frac{t}{L^2}, \quad f_A = \frac{F_A L^3}{EI}, \quad u = \left\{\frac{\rho A}{EI}\right\}^{1/2} UL$$

$$h = \frac{D}{D_h}, \quad \epsilon = \frac{L}{D} \equiv \frac{L}{2a}, \quad c_f = \frac{4}{\pi}C_f \tag{6}$$

leading to

$$\frac{\partial^4 \eta}{\partial \xi^4} + f_A - \tfrac{1}{2}\epsilon c_f u^2(1+h)(1-\xi)\frac{\partial^2 \eta}{\partial \xi^2}$$

$$+\tfrac{1}{2}\epsilon c_f u^2(1+h)\frac{\partial \eta}{\partial \xi} + \tfrac{1}{2}\epsilon c_f \beta^{1/2} u\frac{\partial \eta}{\partial \tau} + (1-\beta)\frac{\partial^2 \eta}{\partial \tau^2} = 0 \tag{7}$$

subject to

$$\eta(0,\tau) = \eta(1,\tau) = \frac{\partial^2 \eta}{\partial \xi^2}\Big|_{\xi=0} = \frac{\partial^2 \eta}{\partial \xi^2}\Big|_{\xi=1} = 0 \tag{8}$$

III. Slender-Body Approximation

According to slender-body theory, the forces on each element of the cylinder may be determined as if that element were part of an infinitely long, rigid cylinder. Hence, one may treat the problem in a much simplified way, because the axial mode shape of the cylinder does not influence the virtual mass of the fluid.

The inviscid aerodynamic forces may be obtained with the aid of the velocity potential

$$\phi = Ux + \phi' \tag{9}$$

where the perturbation potential, $\phi'(r,\theta,t)$, due to small motions of the cylinder, must satisfy

$$\nabla^2\phi' - \frac{1}{c^2}\frac{\partial^2 \phi'}{\partial t^2} = 0 \tag{10}$$

where c is the sonic velocity. This equation must be solved subject to the boundary conditions

$$\frac{\partial \phi'}{\partial r}\Big|_{r=R} = 0 \qquad \text{for } -\infty < x < \infty \tag{11}$$

and

$$\frac{\partial \phi'}{\partial r}\Big|_{r=a} = \left[\frac{\partial v}{\partial t} + U\frac{\partial v}{\partial x}\right]\cos\theta \quad \text{for } 0 \le x \le L$$

$$= 0 \qquad \text{for } x < 0 \text{ and } x > L \tag{12}$$

The perturbation pressure p', due to ϕ', is given by

$$p' = -\rho\frac{\mathrm{D}\phi'}{\mathrm{Dt}} = -\rho\left(\frac{\partial \phi'}{\partial t} + U\frac{\partial \phi'}{\partial x}\right) \tag{13}$$

‡It is noted that this is simplified vis-a-vis that of Ref. 3 by neglecting the viscous force associated with $U = 0$.

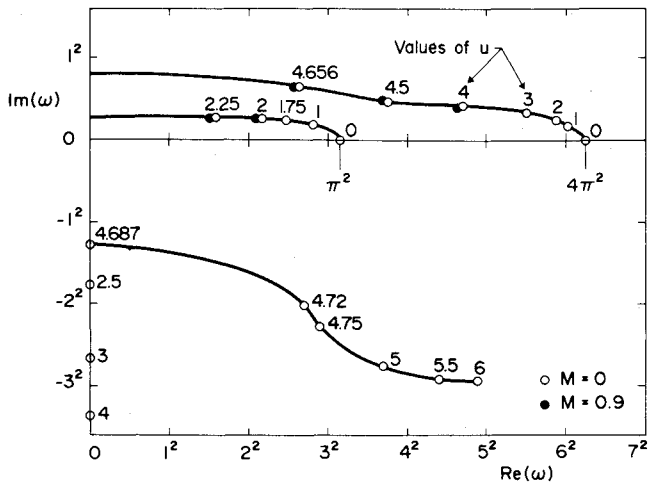

Fig. 2 Argand diagram of the complex frequencies, ω, of the lowest two modes of a pinned-pinned cylinder in bounded compressible flow with the dimensionless flow velocity u as parameter. Results by slender-body approximation. System parameters $\beta=0.1$, $\epsilon c_f=0.5$, $h=1.5$.

and the force on the cylinder in the r direction is given by

$$F_A=\int_0^{2\pi} p'a\cos\theta d\theta \tag{14}$$

Assuming now separable solutions

$$\phi'(r,\theta,t)=B(r)\Theta(\theta)e^{i\Omega t}$$

it is easy to deduce from Eq. (12) that $\Theta(\theta)=\cos\theta$, and the expression for F_A is found to be

$$F_A=-\rho A\frac{B(a)}{aB'(a)}\left(\frac{\partial}{\partial t}+U\frac{\partial}{\partial x}\right)^2 v \tag{15}$$

The expression for $B(a)/B'(a)$ may be found by substituting into Eq. (10), from which one obtains a Bessel equation by changing variables from r to $r^*=\lambda r$, where

$$\lambda a=\Omega a/c \tag{16}$$

is a reduced frequency. This leads to

$$B(r^*)=c_1H_1^1(\lambda r)+c_2H_1^2(\lambda r)$$

where H_1^1 and H_1^2 are Hankel functions of the first and second kind. Finally, applying boundary conditions (11) and (12), one finds

$$\chi\equiv\frac{-B(a)}{aB'(a)}=-\frac{H_1^1(\lambda a)+bH_1^2(\lambda a)}{\lambda aH_0^1(\lambda a)-H_1^1(\lambda a)+b[\lambda aH_0^2(\lambda a)-H_1^2(\lambda a)]} \tag{17}$$

where

$$b=\frac{\lambda RH_0^1(\lambda R)-H_1^1(\lambda R)}{H_1^2(\lambda R)-\lambda RH_0^2(\lambda R)}$$

Hence, according to the slender-body approximation,

$$f_A=\chi\left\{u^2\frac{\partial^2\eta}{\partial\xi^2}+2\beta^{1/2}u\frac{\partial^2\eta}{\partial\xi\partial\tau}+\beta\frac{\partial^2\eta}{\partial\tau^2}\right\} \tag{18}$$

Equation (18) substituted into Eq. (7), with χ given by Eq. (17), is the equation of motion for the system according to this approximation. It was solved by Galerkin's method, utilizing

$$\eta(\xi,\tau)=\sum_{r=1}^{N}\phi_r(\xi)e^{i\omega\tau} \tag{19}$$

with

$$\phi_r(\xi)=\sqrt{2}\sin(r\pi\xi)$$

the normalized eigenfunctions of a pinned-pinned beam. The dimensionless frequency ω, which is generally complex, is related to Ω by

$$\omega=\left\{\frac{\rho A+m}{EI}\right\}^{1/2}\Omega L^2 \tag{20}$$

A special computer program gives the eigenfrequencies ω for any given set of system parameters.

The eigenfrequencies of a typical system, according to a two-comparison function approximation ($N=2$), are shown in Fig. 2, plotted as an Argand diagram. It is noted that small flow velocities damp free motions of the system (i.e., $\mathrm{Im}(\omega)>0$), while the frequencies of oscillation, $\mathrm{Re}(\omega)$, are diminished. For sufficiently high u, the first-mode frequency vanishes, and one branch of its locus crosses to the negative $\mathrm{Im}(\omega)$-axis, indicating the onset of divergence (buckling) at $u\equiv u_{cb}\simeq 2.33$. At higher flow, the second mode is also subject to divergence; then the loci of the two modes coalesce, and one branch leaves the negative $\mathrm{Im}(\omega)$-axis at a point where $\mathrm{Re}(\omega)\neq 0$, indicating the onset of coupled-mode flutter at $u\equiv u_{cf}=4.69$. The *dimensionless* ω and critical values of u are little affected by compressibility, as may be noted by comparing the results for the two different Mach numbers shown, $M=0$ and $M=0.9$.§

The results for an incompressible fluid, as obtained, for example, by the work of Ref. 3, are essentially the same (to within three significant figures) as those for $M=0$ in the figure above. Of course, they should be identical, as for $\lambda a\to 0$ and $\lambda R\to 0$, χ in Eq. (17) simplifies to $\chi=(R^2+a^2)/(R^2-a^2)$, which is the value utilized in Ref. 3; nevertheless, the comparison above is useful in establishing the degree of precision in the numerical evaluation of the Hankel functions.

Finally, the value of u_{cf} obtained here with $N=2$ in Eq. (19) cannot be hoped to be very precise. The reason for utilizing $N=2$ is for ease of comparison with results yet to be obtained, where Galerkin solutions with more terms are rather difficult to accommodate.

IV. Three-Dimensional Approximation

In the previous section, it was seen that the virtual mass of the fluid was dependent on both frequency and flow velocity [Eqs. (16) and (17)]; yet it was independent of axial mode shape in accordance with the slender-body approximation, the virtual mass having been obtained by examining a slice of fluid normal to the cylinder, and ϕ' in Eq. (10) being independent of x. Here an attempt will be made to remove this restriction. Accordingly, the velocity potential still has the form of Eq. (9); similarly, Eqs. (11-14) still hold, but $\phi'=\phi'(x,r,\theta,t)$, and is governed by the equation

$$\nabla^2\phi'-\frac{1}{c^2}\left(\frac{\partial}{\partial t}+U\frac{\partial}{\partial x}\right)^2\phi'=0 \tag{21}$$

§Throughout this paper, the high value of $M=0.9$ is used to establish the degree of dependence on Mach number, although it is realized that for such M, transonic effects, neglected here, may become important.

As before, harmonic time variation will be assumed so that

$$\phi'(x,r,\theta,t)=\bar{\phi}'(x,r,\theta)e^{i\Omega t} \tag{22a}$$

$$v(x,t)=\bar{v}(x)e^{i\Omega t} \tag{22b}$$

Considering next a combination of Gallilean and Lorentz transformations

$$x'=x,\quad r'=r(1-M^2)^{1/2},\quad \theta'=\theta,\quad t'=t+xM/[c(1-M^2)] \tag{23}$$

ϕ' may be written in the form [12]

$$\phi'(x,r',\theta,t)=e^{i\Omega t}e^{ikMx}T(x,r',\theta) \tag{24}$$

where

$$\frac{1}{r'}\frac{\partial}{\partial r'}\left(r'\frac{\partial T}{\partial r'}\right)+\frac{1}{r'^2}\frac{\partial^2 T}{\partial\theta^2}+\frac{\partial^2 T}{\partial x^2}+k^2T=0 \tag{25}$$

is a Helmholtz equation, and k, in reduced-frequency form, is given by

$$ka=\frac{\Omega a}{U}\frac{M}{1-M^2} \tag{26}$$

Several attempts to solve the coupled problem in general, by assuming arbitrary expressions for $\bar{v}(x)$, e.g., as in Eq. (19), and equivalent forms for the x variation of T, have not been successful. Accordingly, an approximate solution will be presented in which, for the purposes of determining the aerodynamic forces, simple sinusoidal axial forms are prescribed for both $\bar{v}(x)$ and $T(x,r',\theta)$,¶ yet for the dynamical analysis of the system, solutions of the form of Eq. (19) are retained. Hence, taking

$$v(x,t)=\sin k_n x\, e^{i\Omega t}\qquad k_n=n\pi/L\qquad n=1,2,\ldots \tag{27}$$

and

$$T(x,r',\theta)=\sin k_n x B(r')\Theta(\theta) \tag{28}$$

and proceeding as in the previous section, it is easily found that $\Theta(\theta)=\cos\theta$ and that $B(r')$ is governed by the Bessel equation

$$\frac{d^2B}{dr'^2}+\frac{1}{r'}\frac{dB}{dr'}+\left(\lambda_n^2-\frac{1}{r'^2}\right)B=0 \tag{29}$$

where

$$\lambda_n a=[(ka)^2-(k_n a)^2]^{1/2} \tag{30}$$

[compare Eq. (16)]. Solution of Eq. (29) has exactly the same form as in the previous section, except that the argument of the Hankel functions is $\lambda_n r$ instead of λr. Similarly, f_A may be written in the same form as Eq. (18), with the dimensionless virtual mass $\chi=-B(a)/[aB'(a)]$ given by Eq. (17), with λ_n substituted for λ.

Calculations with this model, for the same system as in Fig. 2, give closely similar results, as shown in Fig. 3. Here $u_{cb}\simeq 2.34$ and $u_{cf}\simeq 4.70$, for $M=0$ vis-à-vis 2.33 and 4.69 according to the slender-body approximation. Nevertheless,

¶This is consistent with the assumption that fluid perturbations and cylinder motions should have the same axial waveform.

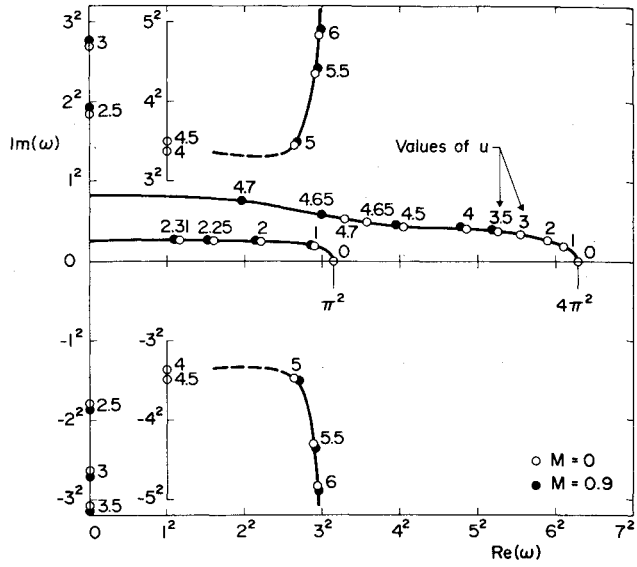

Fig. 3 Argand diagram of the complex frequencies, ω, of the lowest two modes of the same pinned-pinned cylinder system as in Fig. 2. Results obtained by the three-dimensional approximation of Sec. IV. The points on the vertical lines inside the frame of the figure are points on the Im(ω) axis drawn in this manner for compactness.

Table 1 Comparison of the results obtained by the methods of Secs. III and IV, showing the effect of slenderness, ϵ, for $M=0$

Method used in calculations	u_{cb} $\epsilon=20$	u_{cb} $\epsilon=5$	ω_1 $(u=2)$ $\epsilon=20$	ω_1 $(u=2)$ $\epsilon=5$
Slender-body theory of Sec. III	2.33	2.19	$4.72+0.068i$	$3.79+0.017i$
3-D model of Sec. IV	2.34	2.37	$4.81+0.069i$	$5.01+0.020i$

the loci in the two cases are not identical, especially the point on the Argand diagram associated with the onset of coupled-mode flutter.

The similarity in the results obtained by the two methods is easily explained upon examining Eq. (30) more closely. Substituting the expressions for k and k_n in it, and recalling that $\epsilon=L/(2a)$, one obtains

$$\lambda_n a=\left\{\left(\frac{\Omega a}{c}\right)^2-\left(\frac{n\pi}{2\epsilon}\right)^2\right\}^{1/2} \tag{31}$$

It is, therefore, obvious that

$$\lim_{\epsilon\to\infty}\lambda_n a=\frac{\Omega a}{c}=\lambda a \tag{32}$$

retrieving exactly the slender-body approximation, which strictly applies for large L/a.

Now, the results of Figs. 2 and 3 are for $\epsilon=20$ ($L/a=40$), which does correspond to a slender cylinder. It would be of interest to compare slender-body theory to this three-dimensional (3-D) model for a less-than-slender cylinder; e.g., for $\epsilon=5$. The results are summarized in Table 1. It is seen that the numerical values of both u_{cb} and ω_1 at $u=2$ diverge for $\epsilon=5$, whereas they are quite close for $\epsilon=20$, showing that for less-than-slender bodies the theory of Sec. III is not very reliable. It is noted here that slender-body theory predicts a decrease in u_{cb} with decreasing ϵ, reflecting the associated reduction in flow-induced tension, which is proportional to the third and fourth terms involving ϵc_f in Eq. (7), yet presuming constant aerodynamic forces per unit length. In this 3-D model, however, it is seen from Eq. (31), that the

Table 2 Effect of compressibility for slender and nonslender cylinders, according to 3-D model of Sec. IV

M	u_{cb}		ω_1 $(u=2)$	
	$\epsilon=20$	$\epsilon=5$	$\epsilon=20$	$\epsilon=5$
0	2.34	2.37	$4.81+0.069i$	$5.01+0.020i$
0.9	2.33	2.23	$4.72+0.068i$	$3.84+0.016i$

argument of the aerodynamic forces is reduced as ϵ decreases, and this evidently counterbalances the effect of reduction in tension, resulting in a small net increase in u_{cb}.

It is worth stressing that if one wishes to compare the results for different ϵ, one should be constantly aware that in this paper comparisons are made in terms of the *dimensionless* flow velocities and frequencies, u and ω, rather than the *dimensional* U and Ω. Recalling that $u \propto L$ and $\omega \propto L^2$, it is evident that for shorter cylinders both U and Ω will be much higher than for longer ones, irrespective of the relatively small variations of u and ω with ϵ.

Next, it is of interest to examine the effect of compressibility on the dynamics of the system and to compare the results for slender and nonslender cylinders. The values of u_{cb} and ω_1 at $u=2$ are shown in Table 2. It is seen that the effect of compressibility for nonslender bodies is considerably stronger than for slender ones; for example, in terms of critical flow velocities u_{cb}, differences between $M=0$ and $M=0.9$ are of the order of 6-7% for $\epsilon=5$, while they are less than 1% for $\epsilon=20$; the effect on ω is even more pronounced. These effects may be understood once more by examining Eqs. (31) and (32).

All the foregoing pertain to bounded flow geometries. Calculations were also made for a cylinder in unconfined flow. For a system with the same parameters as those of Fig. 3 but $h=0$, the behavior of the system was found to be similar, but the critical flow velocities are much higher ($u_{cb} \simeq 3.39$, $u_{cf} \simeq 7.04$ for $M=0$). As before, the effect of compressibility is very weak for slender cylinders.

Some further study of the problem was conducted where, instead of a standing wave in Eqs. (27) and (28), of axial form $\sin k_n x$, a traveling wave solution was investigated. This will be dealt with separately, however, in Sec. VI.

V. Integral Transform, Generalized-Force Approach

So far, the inviscid aerodynamic forces were derived in two different but approximate ways: one is strictly a slender-body approximation with its inherent limitations; the other involves a 3-D formulation where the inviscid aerodynamic forces were determined under the assumption of a prescribed single-mode vibration of the cylinder in order to render the solutions tractable. Generalization to arbitrary spatial forms, by the methods of Sec. IV at least, appears to render the problem intractable.

Now, an implicit feature of this problem is the continuous and time-dependent interaction of the flowfield on the one hand, and the cylinder deformation field on the other. Hence, it is natural to attempt a less-restricted derivation of the aerodynamic forces—in the sense of their corresponding to arbitrary spatial forms of cylinder deformation—by means of the powerful integral transform techniques which are especially well suited for such problems. Studies of this nature were made by Dowell, who obtained expressions for the generalized aerodynamic forces acting on a cylindrical shell in subsonic or supersonic, internal and external flows, e.g., Ref. 8. In what follows, the formulation will proceed along similar lines, noting nevertheless the added complication here of outer containment of the flow.

Obviously, Eqs. (22) still hold; however, instead of Eqs. (24) and (28), the following forms are introduced

$$\phi'(x,r,\theta,t) = \psi(x,r)\cos\theta e^{i\Omega t} \tag{33}$$

involving arbitrary spatial dependence $\psi(x,r)$. This may be written as an inverse Fourier transform,

$$\psi(x,r) = \frac{1}{2\pi}\int_{-\infty}^{\infty} \psi^*(\alpha,r)e^{-i\alpha x}\mathrm{d}\alpha$$

where α is the Fourier transform variable. Similarly, instead of Eq. (27), let us write

$$v(x,t) = \bar{v}(x)e^{i\Omega t}$$

and

$$\bar{v}(x) = \frac{1}{2\pi}\int_{-\infty}^{\infty} \bar{v}^*(\alpha)e^{-i\alpha x}\mathrm{d}\alpha \tag{34}$$

Transforming next the wave equation (21) into the Fourier domain,

$$\frac{\mathrm{d}^2\psi^*}{\mathrm{d}r^2} + \frac{1}{r}\frac{\mathrm{d}\psi^*}{\mathrm{d}r} - \frac{1}{r^2}\psi^* - \mu^2\psi^* = 0 \tag{35}$$

is obtained, where it was assumed that

$$\lim_{x\to\pm\infty} \psi(x,r) = 0 \quad \text{and} \quad \lim_{x\to\pm\infty} \frac{\mathrm{d}\psi(x,r)}{\mathrm{d}x} = 0$$

and where

$$\mu = \{\alpha^2 - [(\Omega-\alpha U)/c]^2\}^{1/2} \quad \text{or} \quad \mu L = [\bar{\alpha}^2 - M^2(\bar{\alpha}-\kappa)^2]^{1/2}$$

where $\bar{\alpha}=\alpha L$ is the dimensionless Fourier transform variable, and $\kappa=\Omega L/U$ is a new reduced frequency.

The full solution of Eq. (35) is given by

$$\psi^*(\mu r) = c_1 I_1(\mu r) + c_2 K_1(\mu r) \tag{36}$$

where I_1 and K_1 are modified Bessel functions of the first and second kind, respectively.

Substituting next Eq. (33) and Eq. (22b) into boundary conditions (12) and (11) yields, after Fourier transformation,

$$\left.\frac{\mathrm{d}\psi^*(\alpha,r)}{\mathrm{d}r}\right|_{r=a} = (i\Omega - i\alpha U)\bar{v}^*(\alpha) \tag{37}$$

and

$$\left.\frac{\mathrm{d}\psi^*(\alpha,r)}{\mathrm{d}r}\right|_{r=R} = 0 \tag{38}$$

Applying Eqs. (37) and (38) to Eq. (36), one obtains

$$\psi^*(\bar{\alpha},a) = i(\kappa-\bar{\alpha})(aU/L)F(\bar{\alpha})\bar{v}^*(\bar{\alpha}) \tag{39}$$

where

$$F(\bar{\alpha}) = \frac{1}{a\mu}\frac{K_1'(R\mu)I_1(a\mu) - I_1'(R\mu)K_1(a\mu)}{I_1'(a\mu)K_1'(R\mu) - K_1'(a\mu)I_1'(R\mu)} \tag{40}$$

The next step involves the evaluation of the pressure perturbation amplitude. Here it is convenient to define the Fourier transform in terms of the dimensionless $\bar{\alpha}$ and $\xi = x/L$**; that is,

$$\bar{p}^*(\bar{\alpha},r,\theta) = L\int_{-\infty}^{\infty} \bar{p}(\xi,r,\theta)e^{i\bar{\alpha}\xi}\mathrm{d}\xi \tag{41}$$

**Analogous forms for $\psi^*(\bar{\alpha},r)$ and $v^*(\bar{\alpha})$ may similarly be defined.

Hence, the Bernoulli equation (13), under the assumption of simple harmonic motion and after Fourier transformation, becomes

$$\bar{p}^*(\bar{\alpha},r,\theta) = -\rho(i\Omega - i\bar{\alpha})\cos\theta\psi^*(\bar{\alpha},r) \tag{42}$$

Utilizing Eq. (39) and applying the inverse Fourier transform, the pressure perturbation amplitude on an elementary area of the surface of the cylinder is found to be

$$\bar{p}(\xi,a,\theta) = \frac{1}{2\pi}\frac{\rho U^2 a^2}{L^2}\int_{-\infty}^{\infty}(\kappa-\bar{\alpha})^2 F(\bar{\alpha})\bar{v}^*(\bar{\alpha})\cos\theta e^{-i\bar{\alpha}\xi}\,d\bar{\alpha} \tag{43}$$

Integrating this pressure over the circumference of the cylinder yields the amplitude of the aerodynamic force F_A for an arbitrary deformation shape of the cylinder. It will be assumed that this deformation is expressed in terms of suitable comparison functions, $\psi_r(\xi)$, by

$$\eta(\xi,\tau) = \frac{\bar{v}(\xi)}{L}e^{i\Omega t} = \sum_{m=1}^{\infty} A_m\psi_m(\xi)e^{i\omega\tau} \tag{44}$$

Hence, after performing the integration over θ in Eq. (43), the aerodynamic force is found to be

$$F_A(\xi,\tau) = \rho U^2\frac{a^2}{2L^2}e^{i\omega\tau}\int_{-\infty}^{\infty}(\kappa-\bar{\alpha})^2F(\bar{\alpha}) \times\left\{L\int_{-\infty}^{\infty}\sum_{m=1}^{\infty}A_m\psi_m(\xi)e^{i\bar{\alpha}\xi}\,d\xi\right\}e^{-i\bar{\alpha}\xi}\,d\bar{\alpha} \tag{45}$$

Noting that the integral in the brackets reduces to one from 0 to 1, as $\bar{v}(\xi)$ and $\psi_m(\xi)$ are zero elsewhere, the dimensionless aerodynamic force f_A, defined in Eq. (6), may be written as:

$$f_A(\xi,\tau) = \frac{u^2}{2\pi}\int_{-\infty}^{\infty}(\kappa-\bar{\alpha})^2F(\bar{\alpha}) \times\left\{\sum_{m=1}^{\infty}\int_0^1 A_m\psi_m(\xi)e^{i\bar{\alpha}\xi}\,d\xi\right\}e^{-i\bar{\alpha}\xi}\,d\bar{\alpha}e^{i\omega\tau} \tag{46}$$

This together with Eq. (44) when substituted in Eq. (7) is used to solve the problem by Galerkin's method. In this connection, the generalized forces are required and are given by

$$Q_{mr} = \int_0^1 \bar{F}_{A,m}(\xi)\psi_r(\xi)\,d\xi \qquad m,r=1,2,3,\ldots \tag{47}$$

where $\bar{F}_{A,m}$ is the aerodynamic force amplitude due to a deflection $\psi_m(\xi)$; that is,

$$\bar{F}_{A,m}(\xi) = \frac{u^2}{2\pi}\int_{-\infty}^{\infty}(\kappa-\bar{\alpha})^2F(\bar{\alpha})\left\{\int_0^1\psi_m(\xi)e^{i\bar{\alpha}\xi}\,d\xi\right\}e^{-i\bar{\alpha}\xi}\,d\bar{\alpha}$$

Finally, it is convenient to write the generalized forces in the form

$$Q_{mr} = \frac{u^2}{2\pi}\int_{-\infty}^{\infty}F(\bar{\alpha})G_{mr}(\bar{\alpha})\,d\bar{\alpha} \tag{48}$$

where

$$G_{mr}(\bar{\alpha}) = (\bar{\alpha}-\kappa)^2\int_0^1\psi_m(\xi)e^{i\bar{\alpha}\xi}\,d\xi\int_0^1\psi_r(\xi)e^{-i\bar{\alpha}\xi}\,d\xi \tag{49}$$

To evaluate Q_{mr} one has to calculate $G_{mr}(\bar{\alpha})$ first, which presents no difficulties, especially for a cylinder with pinned ends, where $\psi_m(\xi)=\sqrt{2}\sin m\pi\xi$. The integration over $\bar{\alpha}$ in Eq. (48) must be performed carefully, assessing first the existence and location of poles in the integrand. Recalling Eq. (40), separate consideration is given to μ and to the remainder of the denominator:

1) A computer method, based on quadratic fit with deflation,[13,14] was applied to find the roots of $I_1'(a\mu)K_1'(R\mu) - K_1'(a\mu)I_1'(R\mu)$, establishing that its zeros lie off the Re($\bar{\alpha}$) axis.

2) In the case of $\mu=[\bar{\alpha}^2-M^2(\bar{\alpha}-\kappa)^2]^{1/2}/L$, solving for $\bar{\alpha}$ in terms of μ, one has $\bar{\alpha}_{1,2}=[-2\kappa M^2\pm\sqrt{\Delta}]/[2(1-M^2)]$, where $\Delta=4[(\mu L)^2-M^4\kappa^2]$. Assuming a nonzero imaginary part of the frequency, which is perfectly reasonable for the problem at hand, substitution of a complex frequency into κ and thence into $\bar{\alpha}_{1,2}$ shows that $\mu=0$ does not arise.

Hence, the integrand in Eq. (48) will never have poles on the Re($\bar{\alpha}$) axis; that is, normal integration along $\bar{\alpha}$ may safely be performed. Nevertheless, numerical solution of the problem is not trivial, the difficulties arising from the intricate dependence of Q_{mr} on the complex ω. Kornecki,[15] in his work on stability of panels and shells, examined aeroelastic instabilities on the basis of a qualitative analysis of the generalized forces, and has categorized possible classes of solution. Here, following Kornecki's classification, three types of analysis have been undertaken, relating to 1) static stability in compressible steady flow; 2) dynamic stability in incompressible unsteady flow; and 3) dynamic stability in compressible unsteady flow. In class 1, the simplification involves taking $\omega=0$ in the calculation of Q_{mr} and, hence, is strictly valid only at the threshold of buckling, where ω is really zero. Class 2 is essentially a trivial case of 3, which is the most general; the simplification in class 2 arises through $M=0$, so that $F(\bar{\alpha})$ of Eq. (40) is no longer a function of ω.

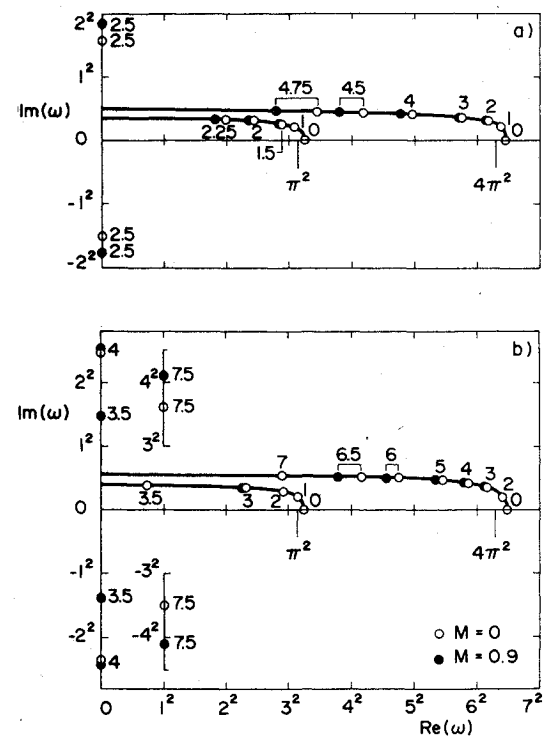

Fig. 4 Argand diagrams of the complex frequencies, ω, of the lowest two modes of a pinned-pinned cylinder in a) bounded flow ($\beta=0.1$, $\epsilon c_f=0.5$, $h=1.5$), and b) in unconfined flow ($\beta=0.1$, $\epsilon c_f=0.5$, $h=0$), with the dimensionless flow velocity, u, as parameter. Results obtained by integral transform generalized-force approach of Sec. V, where the generalized aerodynamic forces have been computed with $\omega=0$. The points on the vertical lines inside the frame of the figure are points on the Im(ω) axis drawn in this manner for compactness.

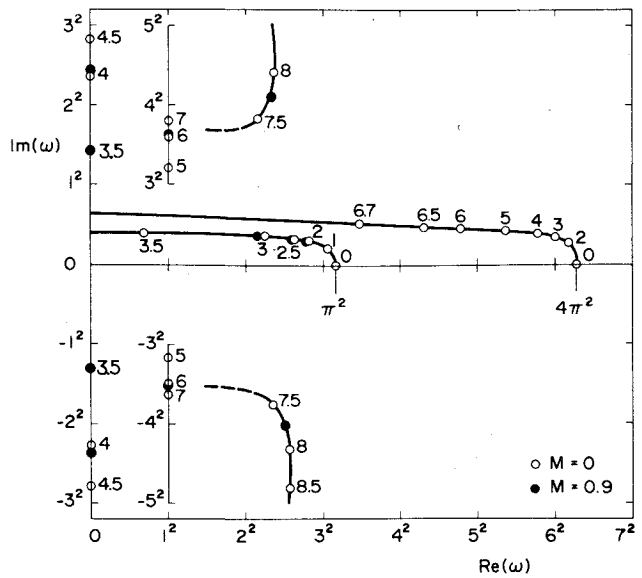

Fig. 5 Argand diagram of the complex frequencies, ω, of the lowest two modes of the pinned-pinned system of Fig. 4b in unconfined flow. Results obtained by the integral transform generalized-force approach of Sec. V, where the generalized aerodynamic forces have been computed in the most general way. The points on the vertical lines inside the figure frame are points on the Im(ω) axis drawn in this manner for compactness.

Typical results for class 1 solutions are shown in Fig. 4, both for bounded and unconfined flow. Considering the bounded flow case first, it is noted that the frequencies at $u=0$ are slightly higher than the correct values ($\omega_1=\pi^2$, $\omega_2=4\pi^2$), as the solution here, by assuming $\omega=0$, renders the aerodynamic forces identically zero at $u=0$; thus, the fluid inertial effect is not taken into account. (This effect is not negligible here, where $\beta=0.1$; it would have been for a very low density fluid, where β would be very small.) The behavior of the system, as shown in Fig. 4a, is similar to that obtained by the other methods except that the eigenfrequencies are slightly higher—an effect disappearing as ω approaches zero. Buckling of the first mode occurs at $u^1_{cb}=2.45$ for $M=0$ and $u^1_{cb}=2.39$ for $M=0.9$. Buckling of the second mode occurs at $u^2_{cb}=4.98$ for $M=0$ and 4.79 for $M=0.9$. However, flutter never arises in this approximation, precisely because the aerodynamic forces are determined with $\omega=0$. It is stressed once more that this class of solution is strictly valid only for $u=u_{cb}$, where, by definition, $\omega=0$. It is noted, nevertheless, that the values of u_{cb} obtained here are somewhat higher than those obtained previously.

The results of Fig. 4b are quite similar, but the dimensionless critical flow velocities and frequencies are higher. Thus, here $u^1_{cb}=3.54$ for $M=0$ and $u^1_{cb}=3.44$ for $M=0.9$

Class 2 and 3 results for the unconfined system are shown in Fig. 5. The frequency-velocity characteristics obtained for the incompressible case—class 2—are within 5% of those obtained by either the slender-body approximation or the three-dimensional model of Sec. IV. This discrepancy in the results is thought to be due to numerical errors, inherent in any integration scheme (here a two-point Gauss scheme) employed in the evaluation of the generalized forces Q_{mr}.

In class 3 solutions, also shown in Fig. 5 for $M=0.9$, the full dependence of Q_{mr} on the frequency ω at any given u is retained. This renders the characteristic equation of the system a highly transcendental equation. Numerical solutions were obtained by a quadratic fit root-seeking procedure. It should be mentioned that in certain cases numerical convergence to the required eigenfrequencies was difficult to achieve, and necessitated both care and the expenditure of considerable computational time. In Sec. VII, these results are compared to those of Sec. IV.

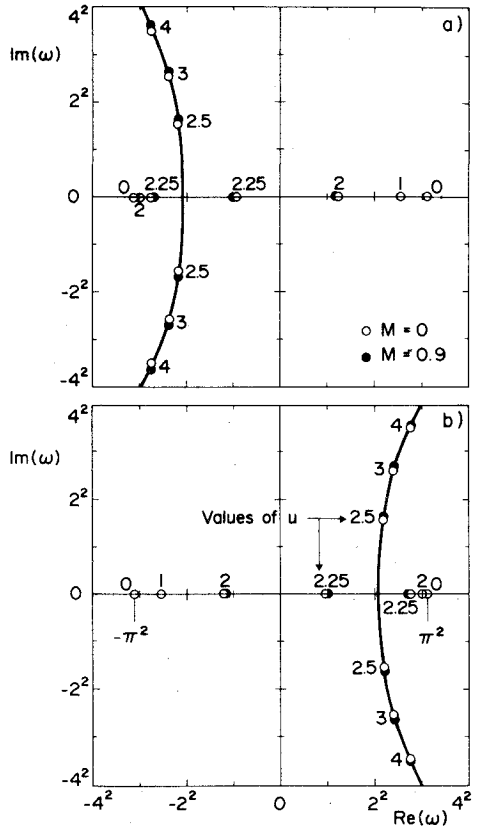

Fig. 6 Argand diagrams of the complex frequencies, ω, of the lowest mode of a laterally unconstrained infinitely long flexible cylinder in bounded axial flow, demonstrating the propagation characteristics of flexural waves, for solutions of the form a) $\eta(\xi,\tau)=\exp(i\omega\tau+i\pi\xi)$ and b) $\eta(\xi,\tau)=\exp(i\omega\tau-i\pi\xi)$. System parameters: $\beta=0.1$, $c_f=0$, $h=1.5$.

VI. Some Comments on Wave Propagation

In this study, it was considered of interest to examine the propagation of flexural waves in the cylinder. For this purpose, the flexible cylinder is considered to be infinitely long and free of all lateral constraints, so that

$$v(x,t)=e^{\pm ik_n x}e^{i\Omega t} \tag{50}$$

Nevertheless, for ease of qualitative comparison to the results presented heretofore, the wavelength is fixed to correspond to an eigenfunction of a pinned-pinned cylinder of length L, so that

$$k_n=n\pi/L \qquad n=1,2,3,\ldots \tag{51}$$

Similarly, instead of the form of Eqs. (22) and (28), the velocity potential ϕ' should now be written as

$$\phi'=e^{ikMx}e^{\pm ik_n x}B(r')\Theta(\theta)e^{i\Omega t} \tag{52}$$

which perfectly satisfies field equation (21).

Proceeding as in Sec. IV, it is found that

$$F_A=\chi\rho A\left(\frac{\partial}{\partial t}+U\frac{\partial}{\partial x}\right)^2 v$$

where χ is as in Eq. (17), but with the argument of the Hankel functions given by Eq. (30) (see the discussion following that equation).

To render the results to be obtained as clear as possible, and also because exact solutions are then possible, all dissipative forces are put to zero. Hence, substituting the above in dimensionless form into Eq. (7) yields

$$\kappa_n^4+\chi u^2\kappa_n^2+2\beta^{1/2}\chi u\omega\kappa_n-[1-\beta(1+\chi)]\omega^2=0 \tag{53}$$

where $\kappa_n = Lk_n = n\pi$, and where it is recalled that χ is a function of ω. For given u and M, this equation was solved by a method of quadratic fit in complex arithmetic.[13,14]

Typical solutions, in Argand-diagram form with u as parameter, are shown in Figs. 6a and 6b, corresponding to solutions $\eta(\xi,\tau) = \exp(i\omega\tau + i\kappa_n\xi)$ and $\exp(i\omega\tau - i\kappa_n\xi)$, respectively, with $\kappa_n = \pi$. Both positive and negative branches of the solution, ω^+ and ω^-, are shown in each case. It is noted that, since all coefficients of Eq. (53) are real, the ω's may be either wholly real or in complex conjugate pairs.

Considering Fig. 6a first, where the waves have been presumed to travel upstream, it is seen that the solution gives both upstream-traveling waves (ω^+ branch) and downstream-traveling waves (ω^- branch). The latter generally have a lower phase velocity, and only at $u=0$ are the two equal, so that an apparently standing wave could then be obtained if both waves are present.

Mathematically, the general solution may be written as:

$$\eta(\xi,\tau) = A_1\exp(i\omega^+\tau + i\kappa_n\xi) + A_2\exp(i\omega^-\tau + i\kappa_n\xi) \quad (54)$$

Writing $\omega^- = -\bar{\omega}_1$ and $\omega^+ = \bar{\omega}_2$, let us consider interfering forward and backward waves of equal amplitude and wavenumber $k_n = \pi$. In this case, Eq. (54) may be written in the form

$$\eta(\xi,\tau) = 2\cos[\tfrac{1}{2}(\bar{\omega}_1 + \bar{\omega}_2)\tau]\exp[i\pi\xi + i\tfrac{1}{2}(\bar{\omega}_2 - \bar{\omega}_1)\tau] \quad (55)$$

This is a wave traveling with frequency $\frac{1}{2}(\bar{\omega}_2 - \bar{\omega}_1)$, with amplitude modulated at a frequency $\frac{1}{2}(\bar{\omega}_2 + \bar{\omega}_1)$. Since $\bar{\omega}_2 - \bar{\omega}_1 < 0$ always (Fig. 6a), the waveform travels downstream.

It is noted that for $u \simeq 2.17$, $\bar{\omega}_2$ vanishes and there exists only a downstream-traveling wave

$$\eta(\xi,\tau) = 2\cos\tfrac{1}{2}\omega_1\tau\,\exp(i\pi\xi - i\tfrac{1}{2}\omega_1\tau)$$

For $u > 2.17$, ω_2 itself becomes negative, so that waves can no longer propagate upstream, but we have two kinds of waves both traveling downstream, with different phase velocities. (Of course, all this applies only to waves of wavenumber π; waves of wavenumber 2π, etc., may still propagate upstream until higher cutoff flow velocities are reached.) For higher flow still, $u \simeq 2.41$, $\bar{\omega}_1$ and $\bar{\omega}_2$ become equal, the loci of ω^- and ω^+ coalesce and bifurcate, the ω's becoming complex conjugate, as shown in Fig. 6a. This signifies that for u higher than $u \simeq 2.41$ waves become amplified, which is directly equivalent to an instability threshold.

Considering Fig. 6b next, it is noted that it is the mirror image of Fig. 6a. Since ω^+ now corresponds to a downstream-traveling wave and ω^- to one traveling upstream, it is evident that exactly the same information is contained in either of the two figures.

The interested reader is referred to the work of Dugundji et al.[16] on subsonic flutter of panels. By comparing the behavior of finite and infinitely long panels, in terms of standing- and traveling-wave analysis, respectively, the authors obtained very interesting results, some bearing remarkable similarity to those discussed here.

VII. Discussion and Conclusion

This paper has dealt with the dynamics of a flexible cylinder in axial, generally bounded, compressible flow. Its principal aim was to establish the effect of compressibility on the dynamical behavior of the system and, especially, on its stability.

Three distinct methods have been pursued for the formulation of the inviscid hydrodynamic forces (which govern the dynamical behavior of the system): a slender-body approximation, a three-dimensional, approximate-differential method, and an integral transform approach which yields the generalized aerodynamic forces directly. The results obtained by all methods, in terms of system eigenfrequencies and critical flow velocities for instability, are qualitatively similar; quantitative differences do exist, as might be expected, partly because of the different physical assumptions and approximations made, and partly because of the numerical schemes adopted in the solution procedures.

The most general and precise analysis presented is that of the integral transform method of Sec. V. Unfortunately, it is also the most complex and most difficult and expensive to apply numerically. Accordingly, unless one requires high precision, one of the other two methods could be used to advantage; for slender cylinders, the slender-body approximation is sufficiently accurate, while for less-than-slender cylinders, the three-dimensional model of Sec. IV may be good enough. As an example, consider the results of Fig. 5 for $M=0.9$; the integral transform method yields $\omega_1 = 7.944 + 0.0685i$ for $u=2$ and $4.725 + 0.122i$ for $u=3$, vis-à-vis $7.869 + 0.0643i$ and $4.405 + 0.115i$ by the method of Sec. IV, which differ by less than 7%.

In Sec. IV, the effect of slenderness on the dynamical characteristics of the system was discussed briefly, and the inadequacy of slender-body theory for nonslender bodies was made clear. This aspect of the dynamics of the system, even in incompressible flow, has not been examined in any of the previous studies, to the best of the authors' knowledge. (Similar discussion relating to the effect of slenderness on the dynamics of cylindrical shells subjected to axial flow may be found in Refs. 8, 17, and 18.)

The effect of compressibility on the dynamics of the system has been shown to be rather weak for slender cylinders. Perhaps this could have been qualitatively predicted on physical grounds. Nevertheless, the quantitative differences between Mach numbers $M=0$ and $M=0.9$ were found to be truly surprisingly small; they are obviously too small to account for the differences in behavior of slender cylinders in incompressible single-phase flow and in compressible two-phase flow discussed in the Introduction. For nonslender cylinders, however, the effect of compressibility becomes more significant, as discussed in Sec. IV. The effect of increased confinement, on the other hand, although severely destabilizing the system, leads to no significant enhancement of the effect of compressibility.

Some very interesting results were obtained relating to flexural wave propagation in infinitely long cylinders subjected to axial flow. It was found that for sufficiently high flow velocity, waves of a given wavelength cannot propagate upstream. Moreover, there exists a threshold flow velocity, beyond which the downstream-propagating waves become amplified, an analogous phenomenon to the flow-induced instabilities obtained for cylinders of finite length. This topic deserves further study.

It should be stressed that the numerical results presented throughout this paper were obtained on the basis of a two-mode Galerkin approximation; accordingly, the second-mode eigenfrequencies are not very precise. This was done for expediency in order to reduce the computational expense, especially for the integral transform method. Further information on this and most other aspects of this work may be found in Ref. 19.

Acknowledgments

This work was supported partly by a research contract from the Chalk River Nuclear Laboratories of Atomic Energy of Canada, and partly from research grants from the Natural Sciences and Engineering Research Council of Canada and the "Programme de formation de chercheurs et d'action concertée" of Québec, to all of whom the authors are grateful.

References

[1] Paidoussis, M. P., "Dynamics of Flexible Slender Cylinders in Axial Flow. Part 1: Theory," *Journal of Fluid Mechanics*, Vol. 26, Dec. 1966, pp. 717-736.

[2]Paidoussis, M. P., "Dynamics of Flexible Slender Cylinders in Axial Flow. Part 2: Experiments," *Journal of Fluid Mechanics,* Vol. 26, Dec. 1966, pp. 737-751.

[3]Paidoussis, M. P., "Dynamics of Cylindrical Structures Subjected to Axial Flow," *Journal of Sound and Vibration,* Vol. 29, Aug. 1973, pp. 365-385.

[4]Paidoussis, M. P., "The Dynamics of Clusters of Flexible Cylinders in Axial Flow: Theory and Experiments," *Journal of Sound and Vibration,* Vol. 65, Aug. 1979, pp. 391-417.

[5]Paidoussis, M. P. and Pettigrew, M. J., "Dynamics of Flexible Cylinders in Axisymmetrically Confined Flow," *Journal of Applied Mechanics,* Vol. 46, March 1979, pp. 37-44.

[6]Carlucci, L. N., "Damping and Hydrodynamic Mass of a Cylinder in Simulated Two-Phase Flow," *Transactions of ASME, Journal of Mechanical Design,* Vol. 102, July 1980, pp. 597-602.

[7]Davies, A. L., "The Speed of Sound in Mixtures of Water and Steam," *Proceedings, Symposium on Two-Phase Flow Dynamics,* Paper 5.2, Session V: Propagation Phenomena, Eindhoven, Sept. 1967.

[8]Dowell, E. H. and Widnall, S. E., "Generalized Aerodynamic Forces on Oscillating Cylindrical Shell: Subsonic and Supersonic Flow," *AIAA Journal,* Vol. 4, April 1966, pp. 607-610.

[9]Dowell, E. H., *Aeroelasticity of Plates and Shells,* Noordhoff International Publishing, Leyden, 1975.

[10]Taylor, G. I., "Analysis of the Swimming of Long and Narrow Animals," *Proceedings of the Royal Society (London),* Series A, Vol. 214, Aug. 1952, pp. 158-183.

[11]Hawthorne, W. R., "The Early Development of the Dracone Flexible Barge," *Proceedings of the Institution of Mechanical Engineers,* Vol. 175, 1961, pp. 52-83.

[12]Küssner, H. G., "General Airfoil Theory," NACA TM 979, 1941.

[13]Muller, D. E., "A Method for Solving Algebraic Equations Using an Automatic Computer," *Mathematical Tables and other Aids to Computation,* Vol. 10, Jan. 1956, pp. 208-215.

[14]Frank, W. L., "Finding Zeros of Arbitrary Functions," *Journal of the Association for Computing Machinery,* Vol. 5, 1958, pp. 154-160.

[15]Kornecki, A., "Static and Dynamic Instability of Panels and Cylindrical Shells in Subsonic Potential Flow," *Journal of Sound and Vibration,* Vol. 32, Jan. 1974, pp. 251-263.

[16]Dugundji, J., Dowell, E., and Perkin, B., "Subsonic Flutter of Panels on Continuous Elastic Foundations," *AIAA Journal,* Vol. 1, May 1963, pp. 1146-1154.

[17]Dowell, E. H. and Widnall, S. E., "Generalized Aerodynamic Forces on an Oscillating Cylindrical Shell," *Quarterly of Applied Mathematics,* Vol. XXIV, April 1966, pp. 1-17.

[18]Matsuzaki, Y. and Kobayashi, S., "Unsteady Supersonic Aerodynamic Forces on an Oscillating Circular Cylindrical Shell," *AIAA Journal,* Vol. 9, Dec. 1971, pp. 2358-2362.

[19]Ostoja-Starzewski, M., "Dynamics of a Single Flexible Cylinder in External Axial Compressible Fluid Flow," M. Eng. Thesis, Dept. of Mechanical Engineering, McGill University, May 1980.